

## Preparation and Application of Co(OH)<sub>2</sub>/Ni-Co LDH as Electrodes in Supercapacitors

Yunlong Zhou<sup>1,3</sup>, Yunsheng Jiang<sup>2</sup>, Zhibiao Hu<sup>1,3</sup>, Xiaoling Lang<sup>1,3,\*</sup>

<sup>1</sup> College of Chemistry and Materials Science, Longyan University, Longyan, Fujian, China 364000

<sup>2</sup> College of Qimai, Longyan University, Longyan, Fujian, China 364000

<sup>3</sup> Fujian Provincial Key Laboratory of Clean Energy Materials, Longyan, Fujian, China 364000

\*E-mail: [ahshio@163.com](mailto:ahshio@163.com)

Received: 21 December 2018 / Accepted: 19 February 2019 / Published: 10 May 2019

---

In this paper, a hydrothermal synthesis method was applied to load Ni-Co Layered Double Hydroxide (LDH) directly on the Nickel foam (NF) as precursor, and by using an electrodeposition method to gain the Co(OH)<sub>2</sub>/Ni-Co LDH composite. The structure and morphology of as-obtained composite was characterized by X-ray diffractometer (XRD) and scanning electron microscopy (SEM). Electrochemical performances of the as-obtained composite were tested by cyclic voltammetry and galvanostatic charge-discharge techniques. The Co(OH)<sub>2</sub>/Ni-Co LDH composite, made by many interconnected nanosheets, was uniformly distributed. The as-obtained electrode achieved a capacity of 825.6 F g<sup>-1</sup> at 1 A g<sup>-1</sup>.

---

**Keywords:** Co(OH)<sub>2</sub>; Ni-Co LDH; supercapacitor; electrodeposition

### 1. INTRODUCTION

As technology advances, diverse energy storage materials are constantly being designed and developed to accommodate the rapid growth of electronic devices and electric vehicles [1, 2]. Supercapacitors have many advantages such as high energy density, fast charge/discharge rate, wide operating temperature range and long cycle life, which make them stand out in many new energy storage devices [3-6].

According to the energy storage mechanism, there are two kinds of supercapacitors, that is double-layer capacitors and pseudocapacitors[7,8]. Double-layer capacitors store electrical energy by electrostatic accumulation on the electrode/electrolyte surface, while pseudocapacitors do that through redox-generated chemical energy. In general, pseudocapacitors have a higher specific capacity than

double-layer capacitors. To date, many materials can be used as pseudocapacitor electrodes, such as transition metal oxides [9], transition metal sulfides [10], hydroxides [11], and conductive polymers.  $\text{Co(OH)}_2$  has great potential as supercapacitor materials. In particular,  $\alpha\text{-Co(OH)}_2$  has drew much attention due to its excellent redox characteristic. Compared with Nickel oxides and hydroxides,  $\text{Co(OH)}_2$  can provide more electrons when conducting redox reactions [12,13].

Layered double hydroxide (LDH), also known as hydrotalcite, is characterized by a wide variety, low raw material prices, and excellent electrochemical performance. The maximum specific capacity of a  $\text{Co}_x\text{Ni}_{1-x}$  LDHs prepared by constant potential deposition was as high as  $2104 \text{ F g}^{-1}$  [14]. However, the samples prepared by this method had a low potential window, only 0.4 V.

In this paper, the  $\alpha\text{-Co(OH)}_2$  is attempted to be supported on Ni-Co LDH with nickel foam as the substrate, thereby improving the problem of insufficient electrochemical performance caused by the low potential window and insufficient crystal layer spacing. The specific operation is as follows: Firstly, a Ni-Co LDH/NF material is prepared by a hydrothermal method as a precursor, and then  $\alpha\text{-Co(OH)}_2$  is attached to the precursor by an electrodeposition method, thereby achieving an improved structure and improving the electrochemical performance.

## 2. EXPERIMENTAL

### 2.1 Ni-Co LDH loaded on nickel foam

One piece ( $3 \text{ cm} \times 6 \text{ cm}$ ) of nickel foam was ultrasonically cleaned with acetone for 15 min and 3 M HCl for 20 min respectively to remove surface impurities and oxides. Finally, it was rinsed repeatedly with deionized water and ethanol.

$\text{Ni(NO}_3)_2 \cdot 6\text{H}_2\text{O}$  (0.5816 g, 2 mmol),  $\text{Co(NO}_3)_2 \cdot 6\text{H}_2\text{O}$  (1.1641 g, 4 mmol) were dissolved in 50 mL of deionized water to form homogeneous solution; The mixture was then transferred into a Teflon-lined stainless steel autoclave. The prepared nickel foam was immersed in the as-obtained solution, sealed and heated to  $150 \text{ }^\circ\text{C}$  for 24 h. After that, the nickel foam loaded with Ni-Co LDH was taken out, washed repeatedly with deionized water and ethanol, and dried to obtain a Ni-Co LDH/NF precursor. The mass of Ni-Co LDH is about  $1.7 \text{ mg} \cdot \text{cm}^{-2}$ .

### 2.2 Electrodeposition of $\text{Co(OH)}_2$ on the precursor

$\text{Co(OH)}_2$  was prepared by electrodeposition on a Ni-Co LDH-loaded nickel foam via an electrochemical workstation (CHI600C, Shanghai CH Instruments Co., Ltd., China).

In a three-electrode system, a Ni-Co LDH/NF precursor ( $1 \text{ cm} \times 1 \text{ cm}$ ) was used as a working electrode, a saturated calomel electrode (SCE) as a reference electrode, and a platinum plate ( $1 \text{ cm} \times 1 \text{ cm}$ ) as a counter electrode. The electrodeposition solution was  $\text{Co(NO}_3)_2 \cdot 6\text{H}_2\text{O}$  (50 mL 10 mM). A current-time curve technique was set up with an initial potential of -1 V and electrodeposition for 10 min at room temperature. The as-obtained  $\text{Co(OH)}_2/\text{Ni-Co LDH}$  composite was rinsed again and again

with deionized water and ethanol and dried. The mass loading of  $\text{Co(OH)}_2$  is about  $4.9 \text{ mg}\cdot\text{cm}^{-2}$ , thus the all active mass is about  $6.6 \text{ mg cm}^{-2}$ .

$\alpha\text{-Co(OH)}_2$  is green [15], while  $\beta\text{-Co(OH)}_2$  is pink. In order to verify that the  $\text{Co(OH)}_2$  prepared by this method is  $\alpha$ -type,  $\text{Co(OH)}_2$  is electrodeposited again with the Nickel foam without Ni-Co LDH, and the color of the obtained product is green; the previously prepared  $\text{Co(OH)}_2/\text{Ni-Co LDH}$  also appears dark green, so it can be confirmed that the electrodeposited  $\text{Co(OH)}_2$  is indeed  $\alpha$ -type.

### 2.3 Material Characterization

The structure of the sample was analyzed by an X-ray diffractometer (DX-2700, Dandong Fangyuan Instrument Co., Ltd., China), and the surface morphology of the sample was characterized by a scanning electron microscope (HITACHI S-3400N) equipped with an energy dispersive spectroscopy (EDS).

### 2.4 Electrochemical Measurements

Cyclic voltammetry (CV), galvanostatic charge-discharge (GCD), and electrochemical impedance spectra (EIS) were performed via a electrochemical workstation, and cycling stability was tested in the Neware Battery Tester. The electrolyte in all measurements was set to 2 M KOH. CV had a voltage range of 0 - 0.7 V and scan speeds of  $10 \text{ mV s}^{-1}$ ,  $20 \text{ mV s}^{-1}$ ,  $30 \text{ mV s}^{-1}$ ,  $40 \text{ mV s}^{-1}$ , and  $50 \text{ mV s}^{-1}$ , respectively. The GCD tests were conducted by a chronopotentiometry technique. The potential window was set to 0.45 V and the current densities were  $1 \text{ A g}^{-1}$ ,  $2 \text{ A g}^{-1}$ ,  $3 \text{ A g}^{-1}$ ,  $4 \text{ A g}^{-1}$ , and  $5 \text{ A g}^{-1}$ , respectively. EIS were measured in a frequency ranging from  $10^{-2} \text{ Hz}$  to  $10^5 \text{ Hz}$ .

## 3. RESULTS AND DISCUSSION

### 3.1 Structural and morphological of $\text{Co(OH)}_2/\text{Ni-Co LDH/NF}$ and $\text{Ni-Co LDH/NF}$

Fig. 1 shows SEM images of  $\text{Co(OH)}_2/\text{Ni-Co LDH/NF}$  and  $\text{Ni-Co LDH/NF}$ . It can be observed that Ni-Co LDH exhibits staggered nanosheets at high magnification (Fig. 1c), which is typical of hydroxalcalite-like structures. Under low magnification (Fig. 1d), it can be evidently shown that the nickel foam skeleton is wrapped by Ni-Co LDH and distributed evenly in every part. Fig. 1a and Fig. 1b are images of  $\text{Co(OH)}_2/\text{Ni-Co LDH/NF}$ . Since  $\alpha\text{-Co(OH)}_2$  is also a hydroxalcalite-like structure, it continues to crystallize into a staggered, sheet-like structure on the original Ni-Co LDH. Compared with Ni-Co LDH/NF, the monolayer of  $\text{Co(OH)}_2/\text{Ni-Co LDH/NF}$  is much thicker and more closely packed with adjacent sheets, resulting in improved electrochemical performance.

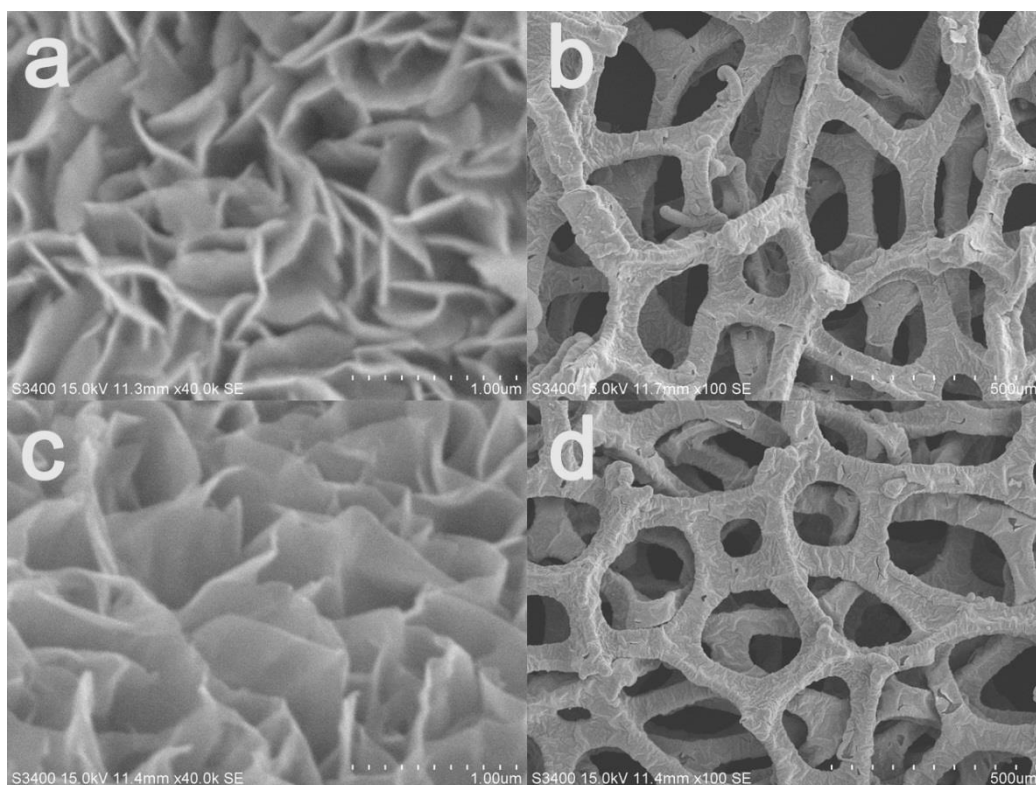


**Figure 1.** SEM images of Co(OH)<sub>2</sub>/Ni-Co LDH/NF (a, b) and Ni-Co LDH/NF (c, d)

Ni-Co LDH prepared by this method is a mixture of Ni(OH)<sub>2</sub> and Co(OH)<sub>2</sub> mixed with  $\alpha$ -type and  $\beta$ -type. Also, it is very difficult to distinguish between Ni(OH)<sub>2</sub> and Co(OH)<sub>2</sub>, because they have nearly the same structure, and their XRD patterns (Fig. 2) of diffraction peaks are located very close to each other, almost coincident [16]. A comparison with the JCPDS 41-1447 and JCPDS 30-0443 cards shows that both of the resulting samples contain Ni(OH)<sub>2</sub> and Co(OH)<sub>2</sub>, and the locations of the standard diffraction peaks of the two JCPDS cards are also very close. In Fig. 2, diffraction peaks appearing at  $2\theta$  of approximately 44.8°, 52.2°, and 76.9° come from the nickel foam substrate.

The difference between the  $\alpha$ -type and the  $\beta$ -type lies in the arrangement of the crystal layer spacing on the C-axis. The crystal layer spacing of the  $\beta$ -Ni(OH)<sub>2</sub> and  $\beta$ -Co(OH)<sub>2</sub> is 4.6 Å on the C-axis [17], without any other spacers; but  $\alpha$ -Ni(OH)<sub>2</sub> and  $\alpha$ -Co(OH) crystal layers are arranged at random, and water molecules form hydrogen bonds with their hydroxyl groups. Therefore, the average crystal layer spacing of  $\alpha$ -Ni(OH)<sub>2</sub> and  $\alpha$ -Co(OH)<sub>2</sub> is about 8 Å. Since the arrangement of the  $\alpha$ -type hydroxides is more disordered and the distance between the crystal layers is larger, and water molecules and other anions are contained, in theory, the electrochemical performance of the composite can be enhanced by re-adhering  $\alpha$ -Co(OH)<sub>2</sub> to the precursor by electrodeposition.

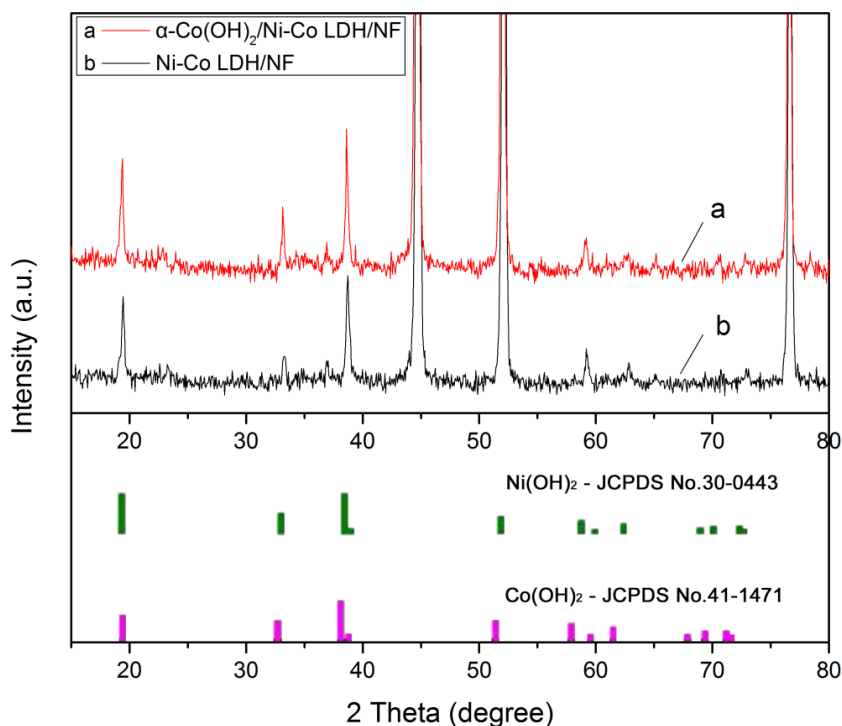


**Figure 2.** XRD patterns of  $\text{Co(OH)}_2/\text{Ni-Co LDH/NF}$  and  $\text{Ni-Co LDH/NF}$  and comparison with JCPDS cards

Table 1 shows the results of the analysis of the atomic percentages of cobalt, nickel, oxygen and carbon of  $\text{Co(OH)}_2/\text{Ni-Co LDH/NF}$ ,  $\text{Ni-Co LDH/NF}$ , and nickel foam (NF) via EDS. The carbon in the table is a byproduct of the nickel foam process.

**Table 1.** the atomic percentages of cobalt, nickel, oxygen and carbon

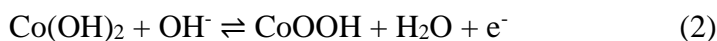
Samples	Co (atomic %)	Ni (atomic %)	O (atomic %)	C (atomic %)
Nickel foam	/	83.96	3.33	11.68
Ni-Co LDH/NF	8.66	25.24	56.92	8.35
$\text{Co(OH)}_2/\text{Ni-Co LDH/NF}$	26.43	7.79	57.04	7.77

It shows that the content of cobalt produced by electrodeposition is much larger than that of the original  $\text{Ni-Co LDH/NF}$ . According to Ma et al [12], the electrochemical properties of cobalt oxides and hydroxides are better than those of nickel.

### 3.2 Electrochemical evaluation

In order to better highlight the electrochemical performance of the  $\text{Co(OH)}_2/\text{Ni-Co LDH/NF}$  composite electrode, most of the experimental data in this paper are directly compared with  $\text{Ni-Co LDH/NF}$ .

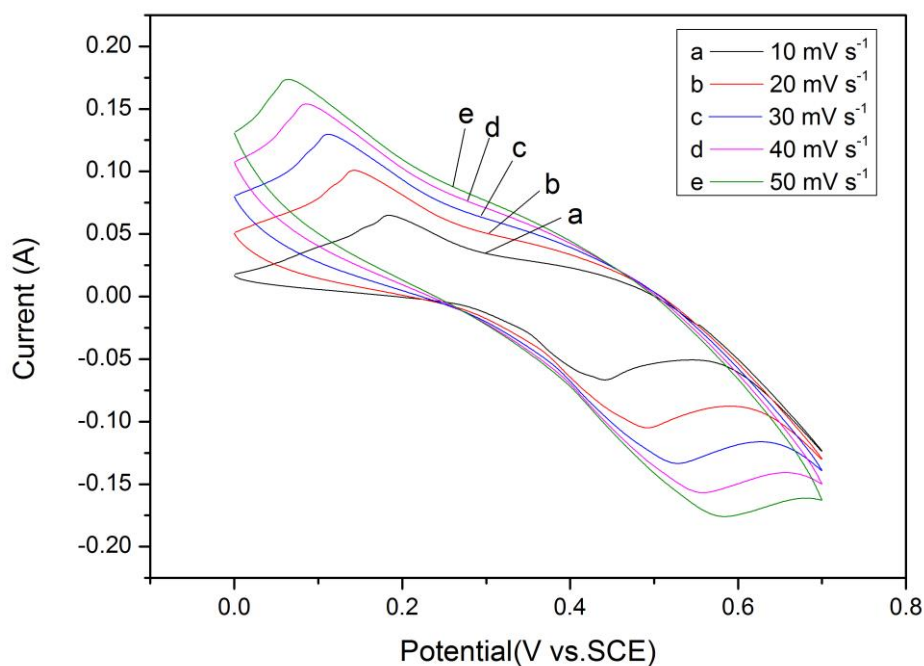
Fig. 3 shows the CV curves of Ni-Co LDH/NF at different scan rates (10-50  $\text{mV s}^{-1}$ ). As the scan rate increases, the closed areas of the curves gradually increase, and the redox peak can be clearly observed.  $\text{Ni(OH)}_2$  and  $\text{Co(OH)}_2$  have the following redox reactions in KOH solution <sup>[18]</sup>:



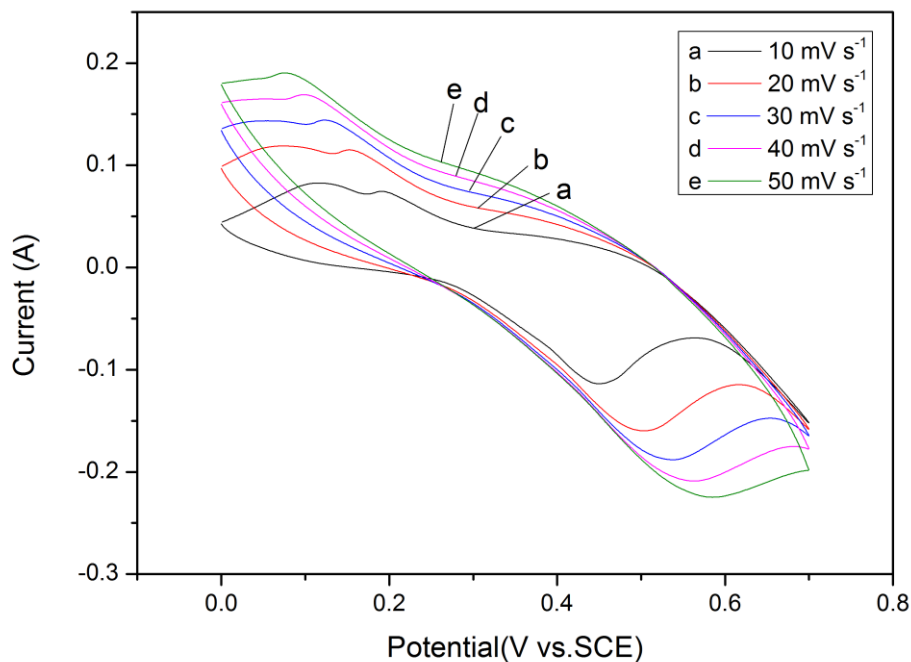
In Fig. 3, the positions of redox peaks do not show a deformation phenomenon with the increase of the scanning rate, indicating that the electron transport and separation in the KOH solution was very stable.

Fig. 4 shows the CV curves of  $\text{Co(OH)}_2/\text{Ni-Co LDH/NF}$  composite electrodes at different scan rates (10-50  $\text{mV s}^{-1}$ ). With the increase of scan rate, closed areas of CV curves of  $\text{Co(OH)}_2/\text{Ni-Co LDH/NF}$  gradually increases, and redox peaks can be clearly observed in the graph because of redox reactions. In Fig. 4, the positions of redox peaks do not appear to be deformed as the scan rate increases, indicating that the electron transport and separation in the KOH solution was also very stable.

Fig. 5 compares the CV curves of Ni-Co LDH/NF and  $\text{Co(OH)}_2/\text{Ni-Co LDH/NF}$  at the same scan rate (50  $\text{mV s}^{-1}$ ). The closed area of  $\text{Co(OH)}_2/\text{Ni-Co LDH/NF}$  is slightly larger than that of Ni-Co LDH/NF, indicating that the electrodeposited  $\alpha\text{-Co(OH)}_2$  can effectively increase the chemical properties of Ni-Co LDH precursor.



**Figure 3.** CV curves of Ni-Co LDH/NF at different scan rates



**Figure 4.** CV curves of Co(OH)<sub>2</sub>/Ni-Co LDH/NF at different scan rates

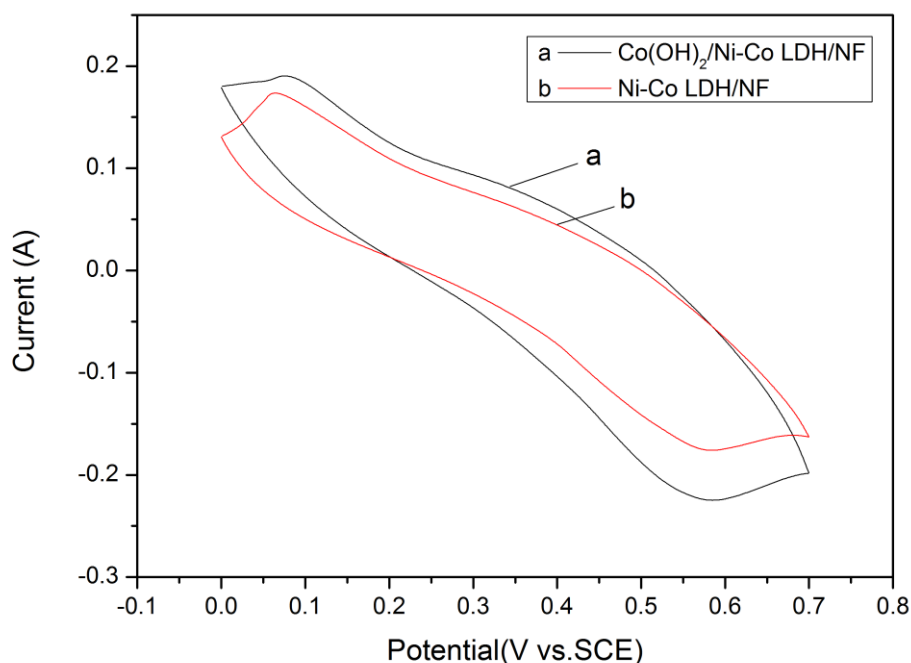


**Figure 5.** CV curves of Co(OH)<sub>2</sub>/Ni-Co LDH/NF and Ni-Co LDH/NF at a scan rate of 50 mV s<sup>-1</sup>

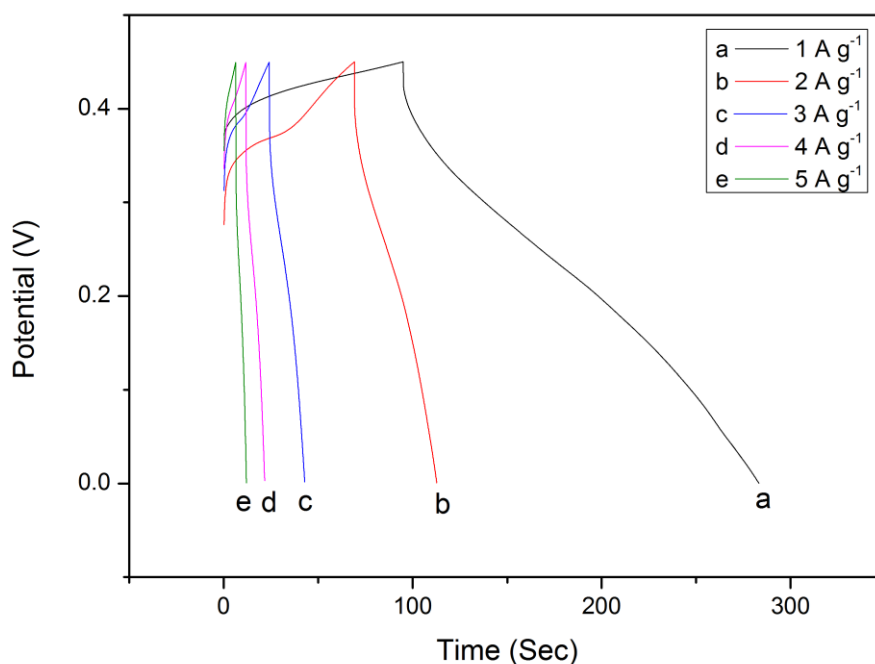
Fig. 6 shows the GCD curves of Ni-Co LDH/NF at different current densities (1-5 A g<sup>-1</sup>). The potential window is 0.45 V. From the experimental data, it can be observed that during the charging process of Ni-Co LDH/NF electrode, the voltage gradually rises to 0.45 V, and a significant plateau

phase appears in the charging curve; during the discharging process, the potential gradually decreases to 0 over time but the plateau phase is not obvious. The specific capacity is calculated as follows:

$$C_s = \frac{I \times \Delta t}{m \times \Delta V} \quad (4)$$

In the formula,  $C_s$  ( $F g^{-1}$ ) is the specific capacitance,  $I$  (A) is the charge and discharge current,  $\Delta t$  (s) is the discharge time, and  $m$  (g) is the active mass involved in charge and discharge at the working electrode.  $\Delta V$  (V) is the potential window.

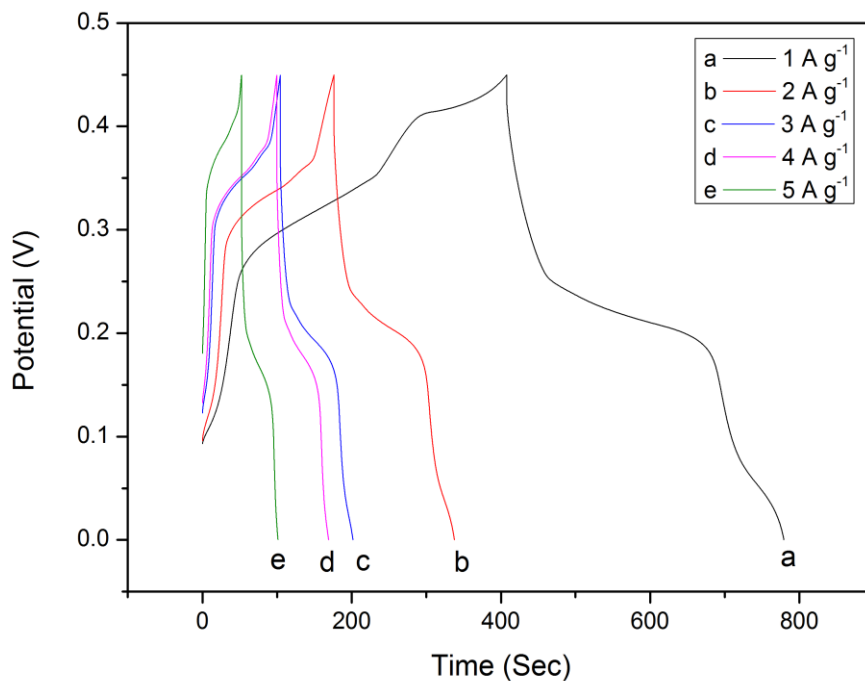
At a current density of  $1 A g^{-1}$ , the specific capacity of the Ni-Co LDH/NF electrode is approximately  $418.7 F g^{-1}$ . As the current density increases, the specific capacity tends to decrease, which is common in supercapacitor materials. At low current densities, ions in the electrolyte can diffuse well around the electrode, increasing the specific capacity; while at high current densities, ions in the electrolyte can only be absorbed by the active materials of the outer layer, which reduce the specific capacity [19].



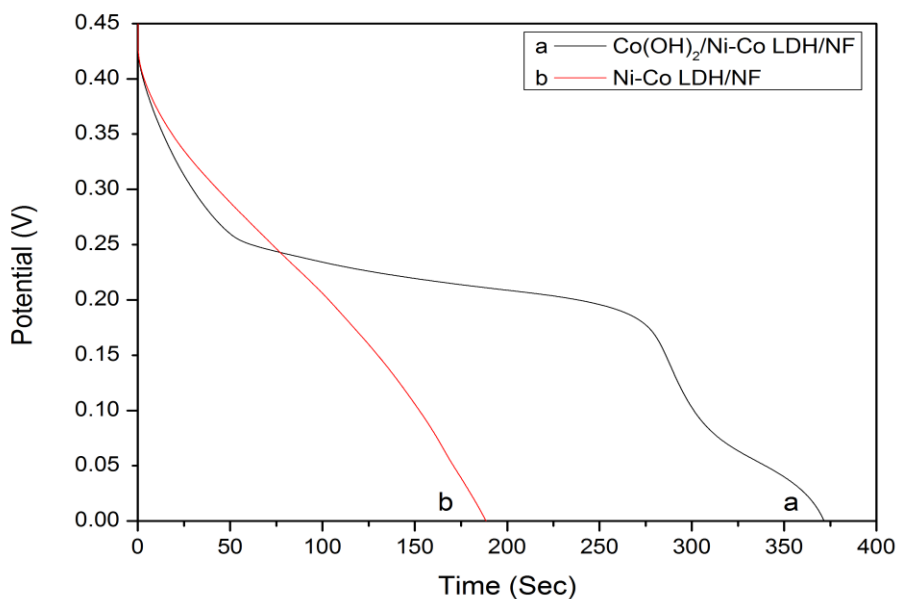
**Figure 6.** GCD curves of Ni-Co LDH/NF at different current densities ( $1 \sim 5 A g^{-1}$ )

Fig. 7 shows the GCD curves of  $Co(OH)_2/Ni-Co$  LDH/NF electrodes at different current densities ( $1 \sim 5 A g^{-1}$ ). The potential window is 0.45 V. From the experimental data, it can be observed that during the charging process of  $Co(OH)_2/Ni-Co$  LDH/NF composite electrode material, the voltage gradually rises to 0.45 V, and the charging curve appears a very obvious plateau period; during the discharge process, the curve decreases slowly, also the plateau period can be clearly observed, indicating that the material is a pseudocapacitor. According to the formula (4), it can be calculated that the specific capacitance of the  $Co(OH)_2/Ni-Co$  LDH/NF composite is approximately  $825.6 F g^{-1}$  at  $1 A g^{-1}$ . Fig. 8 is a comparison of the discharge curves of  $Co(OH)_2/Ni-Co$  LDH/NF and Ni-Co LDH/NF at

1 A g<sup>-1</sup>. The discharge speed of Co(OH)<sub>2</sub>/Ni-Co LDH/NF was slightly faster than Ni-Co LDH/NF at the initial stage, but a considerable plateau appeared in the middle period, which caused a significant slowdown of the discharge rate. The capacitance ratio approaches 2:1, showing that Co(OH)<sub>2</sub>/Ni-Co LDH/NF has better performance.



**Figure 7.** GCD curves of Co(OH)<sub>2</sub>/Ni-Co LDH/NF at different current densities (1 ~ 5 A g<sup>-1</sup>)



**Figure 8.** Comparison of GCD Discharge Curves of Co(OH)<sub>2</sub>/Ni-Co LDH/NF and Ni-Co LDH/NF at 1 A g<sup>-1</sup>

The comparison of Co(OH)<sub>2</sub>/Ni-Co LDH in the work with that of the previously reported electrode materials is listed in Table 2. It shows that the specific capacitance of our Co(OH)<sub>2</sub>/Ni-Co LDH electrode is superior to some other forms of Nickel and/or Cobalt metal oxides, hydroxides, LDHs and so forth.

**Table 2.** Comparison of the electrochemical performance between different electrode materials

Electrode Material	Specific Capacitance	Electrolyte	Ref.
Co(OH) <sub>2</sub> /Ni-Co LDH	825.6 F g <sup>-1</sup> at 1 A g <sup>-1</sup>	2M KOH	This work
Graphene/Ni-Al LDH	213.57 F g <sup>-1</sup> at 1 A g <sup>-1</sup>	1M Na <sub>2</sub> SO <sub>4</sub>	[20]
Ni-Fe LDH (Ni : Fe = 4 : 1)	168 F g <sup>-1</sup> at 1.5 A g <sup>-1</sup>	6M KOH	[21]
Co-Fe LDH	728 F g <sup>-1</sup> at 1 A g <sup>-1</sup>	2M KOH	[22]
Co(OH) <sub>2</sub> /Ni(OH) <sub>2</sub> (Co : Ni = 3 : 1)	104 F g <sup>-1</sup> at 1 A g <sup>-1</sup>	3M KOH	[23]
α-Ni(OH) <sub>2</sub>	562 F g <sup>-1</sup> at 1 A g <sup>-1</sup>	2M KOH	[24]
α-Co(OH) <sub>2</sub>	642.5 F g <sup>-1</sup> at 1 A g <sup>-1</sup>	2M KOH	[25]
NiCo <sub>2</sub> O <sub>4</sub>	437 F g <sup>-1</sup> at 1 A g <sup>-1</sup>	3M KOH	[26]
Co <sub>3</sub> O <sub>4</sub> @ NiCo <sub>2</sub> O <sub>4</sub>	672 F g <sup>-1</sup> at 1 A g <sup>-1</sup>	2M KOH	[27]
NiCo <sub>2</sub> O <sub>4</sub> @ Graphene	778 F g <sup>-1</sup> at 1 A g <sup>-1</sup>	2M KOH	[28]

Excellent electrochemical performance of Co(OH)<sub>2</sub>/Ni-Co LDH can be attributed to the advantages of the cluster structure of the hydroxides. Co(OH)<sub>2</sub> interconnected with Ni-Co LDH can shorten the diffusion distance of ions and form the opening space to store enough power for chemical reaction. Many evenly distributed flakes on the surface of Co(OH)<sub>2</sub> can enlarge the surface area and ensure the electrolyte easily infiltrate into materials. The electrodeposition method of growing materials on the Nickel foam can avoid the use of binder which will greatly decrease internal resistance. Moreover, the flower-like Co(OH)<sub>2</sub>/Ni-Co LDH can introduce multiple Co<sup>2+</sup> ions which will react with electrolyte and bring the extra specific capacity. Hence one can see that Co(OH)<sub>2</sub>/Ni-Co LDH double-layered composites grown on Nickel foam are a kind of promising electrode material for high performance supercapacitors.

The EIS uses a frequency of 100 kHz to 0.01 Hz and set amplitude of 5 mV. Fig. 9 shows a comparison of the EDS of Co(OH)<sub>2</sub>/Ni-Co LDH/NF and Ni-Co LDH/NF. In the high frequency region, the smaller the radius of the semicircle presented by the curve, the lower the resistance to charge-transfer [29]. It can be clearly observed that the semicircle of the high-frequency region of the Co(OH)<sub>2</sub>/Ni-Co LDH/NF electrode is very small and negligible, while the radius of the semicircle of the Ni-Co LDH/NF electrode material is relatively obvious. In the low-frequency region, the slope of

the curve can reflect the Warburg Impedance and the diffusion rate of the electrolyte ions around the active materials [30]. The slope of the low frequency region of the  $\text{Co}(\text{OH})_2/\text{Ni-Co LDH/NF}$  spectrum is significantly larger than that of  $\text{Ni-Co LDH/NF}$ , indicating that the electrode material has a better ion diffusion rate.

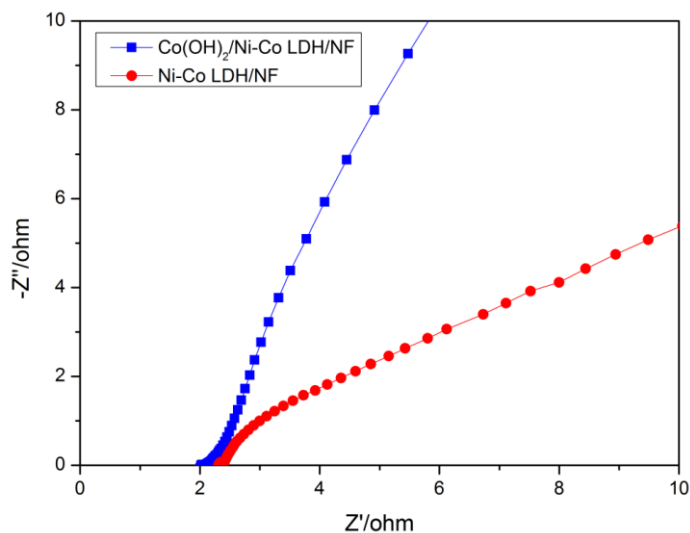


**Figure 9.** Comparison of EIS of  $\text{Co}(\text{OH})_2/\text{Ni-Co LDH/NF}$  and  $\text{Ni-Co LDH/NF}$

#### 4. CONCLUSION

In this paper,  $\text{Ni-Co LDH/NF}$  precursors were prepared by hydrothermal method. On this basis, electrodeposited  $\text{Co}(\text{OH})_2/\text{Ni-Co LDH/NF}$  composite was obtained. The as-obtained product was proved to be a LDH structure containing cobalt and nickel by SEM, EDS and XRD, and the distribution of microstructure of the hydrotalcite-like nanosheets was distributed evenly. Through the analysis and comparison of the samples' CV, GCD, EIS curves and cyclic performance, it can be proved that the  $\text{Co}(\text{OH})_2/\text{Ni-Co LDH/NF}$  composite has a more excellent electrochemical performance. In the case of  $1 \text{ A g}^{-1}$ , the specific capacity of  $\text{Co}(\text{OH})_2/\text{Ni-Co LDH/NF}$  is nearly doubled compared to  $\text{Ni-Co LDH/NF}$ , reaching  $825.6 \text{ F g}^{-1}$ ; compared to other reported Nickel-related or Cobalt-related compound electrodes,  $\text{Co}(\text{OH})_2/\text{Ni-Co LDH/NF}$  in this work shows a more robust electrochemical performance.

#### ACKNOWLEDGEMENT

The authors thank from Fujian Provincial Key Laboratory of Clean Energy Materials, the Cultivation Program of National Natural Science Foundation (LG2014011), the School Research Program of LongYan University (LC2013008), The young and middle-aged project of education department of Fujian Province (JAT170566) and the Science and Technology Key Project of Fujian Province (2015H61010066).

## References

1. Z. Zhang, C. Gao, Z. Wu, W. Han, Y. Wang, W. Fu, X. Li, and E. Xie, *Nano Energy*, 19 (2016) 318.
2. P. Yang, P. Sun, and W. Mai, *Mater. Today*, 19 (2016) 394.
3. C. Portet, P.L. Taberna, P. Simon, E. Flahaut, and C. Laberty-Robert, *Electrochim. Acta*, 50 (2005) 4174.
4. A. Balducci, W.A. Henderson, M. Mastragostino, S. Passerini, P. Simon, and F. Soavi, *Electrochim. Acta*, 50 (2005) 2233.
5. D. Guo, Y. Luo, X. Yu, Q. Li, and T. Wang, *Nano Energy*, 8 (2014) 174.
6. D.P. Dubal, O. Ayyad, V. Ruiz, and C. Gomez-Romero, *Chem. Soc. Rev.*, 44 (2015) 1777.
7. T. Nguyen, M. Boudard, M.J. Carmezim, and M.F. Montemor, *Energy*, 126 (2017) 208.
8. L. Xu, Y. Zhao, J. Lian, Y. Xu, J. Bao, J. Qiu, L. Xu, H. Xu, M. Hua, and H. Li, *Energy*, 123 (2017) 296.
9. D. Xiang, L. Yin, C. Wang, and L. Zhang, *Energy*, 106 (2016) 103.
10. S. Dou, L. Tao, J. Huo, S. Wang, and L. Dai, *Energy Environ. Sci.*, 9 (2016) 1320.
11. J. Chen, J. Xu, S. Zhou, N. Zhao, and C.P. Wong, *J. Mater. Chem. A*, 3 (2015) 17385.
12. H. Ma, J. He, D.B. Xiong, J. Wu, Q. Li, V. Dravid, and Y. Zhao, *ACS Appl. Mater. Interfaces*, 8 (2016) 1992.
13. T. Li, G.H. Li, L.H. Li, L. Liu, Y. Xu, H.Y. Ding, and T. Zhang, *ACS Appl. Mater. Interfaces*, 8 (2016) 2562.
14. V. Gupta, S. Gupta, and N. Miura, *J. Power Sources*, 175 (2008) 680.
15. J.P. Cheng, L. Liu, J. Zhang, F. Liu, and X.B. Zhang, *J. Electroanal. Chem.*, 722 (2014) 23.
16. Z.A. Hu, Y.L. Xie, Y.X. Wang, H.Y. Wu, Y.Y. Yang, and Z.Y. Zhang, *Electrochim. Acta*, 54 (2009) 2737.
17. L. Guerlou-Demourgues, C. Denage, and C. Delmas, *J. Power Sources*, 52 (1994) 269.
18. X. Bai, Q. Liu, H. Zhang, J. Liu, Z. Li, X. Jing, Y. Yuan, L. Liu, and J. Wang, *Electrochim. Acta*, 215 (2016) 492.
19. L. Luo, B. He, W. Kong, and Z. Wang, *J. Alloys Compd.*, 705 (2017) 349.
20. Z. Wang, X. Zhang, J. Wang, L. Zou, Z. Liu, and Z. Hao, *J. Colloid Interface Sci.*, 396 (2013) 251.
21. S. Sanati, and Z. Rezvani, *Ultrason. Sonochem.*, 48 (2018) 199.
22. K. Ma, J.P. Cheng, J. Zhang, M. Li, F. Liu, and X. Zhang, *Electrochim. Acta*, 198 (2016) 231.
23. X. Li, R. Ding, W. Shi, Q. Xu, D. Ying, Y. Huang, and E. Liu, *Electrochim. Acta*, 265 (2018) 455.
24. P.E. Lokhande, K. Pawar, and U.S. Chavan, *Mater. Sci. Energy Technol.*, 1 (2018) 166.
25. J. Jiang, J. Liu, R. Ding, J. Zhu, Y. Li, A. Hu, X. Li, and X. Huang, *ACS Appl. Mater. Interfaces*, 3 (2010) 99.
26. J. Pu, F. Cui, S. Chu, T. Wang, E. Sheng, and Z. Wang, *ACS Sustainable Chem. Eng.*, 2 (2013) 809.
27. X. Gao, Y. Zhang, M. Huang, F. Li, C. Hua, L. Yu, and H. Zheng, *Ceram. Int.*, 40 (2014) 15641.
28. Y. Wei, S. Chen, D. Su, B. Sun, J. Zhu, and G. Wang, *J. Mater. Chem. A*, 2 (2014) 8103.
29. D. Qu, and H. Shi, *J. Power Sources*, 74 (1998) 99.
30. Z. Gu, H. Nan, B. Geng, and X. Zhang, *J. Mater. Chem. A*, 3 (2015) 12069.